Position-Commanding Anti-Sway Controller for 2-D Overhead Cranes Under Velocity and Acceleration Constraints

Ryo Nishimoto and Ryo Kikuuwe

Abstract—This paper proposes an anti-sway controller for two-dimensional overhead cranes. The controller is of the position-commanding type, i.e., it sends position commands to the position-controlled trolley, and it uses the sensor information of the payload sway angle. The position commands are determined so that the trolley tracks the desired position signal sent from an upper-level controller and also so that the payload sway is damped. The sway damping is realized by a leaky integral controller, which employs a high-pass filtered time integral of the sway angle. In addition, arbitrary limits can be imposed on the first and second derivatives of the position command, and thus it is applicable to cases where the desired position signal from the upper-level controller is nonsmooth or discontinuous. Due to these features, the controller is expected to be useful in both human-operated and autonomous systems. The controller was validated with a laboratory setup. This paper also presents an algorithm that can be attached to the proposed controller to prevent the overshoot, which can take place when the desired position signal is discontinuous.

Index Terms—Overhead crane, Position command, Anti-sway control, Velocity limits, Acceleration limits

I. INTRODUCTION

Suppression of the payload sway of overhead cranes is an important issue in many industry sectors such as logistics, warehousing, manufacturing, and construction [1]. For automatic cranes, input shaping techniques are widely used [2]–[5], in which the trolley is position-controlled to track predefined trajectories that are carefully designed not to excite the sway of the payload. This approach is not straightforward to apply to cranes manually operated by human operators because the position command from the human operator is intrinsically unpredictable. In addition, input shaping techniques are not suited to cope with disturbances such as wind and collisions. To deal with such unpredictable factors, control techniques employing appropriate sensor feedback are necessary.

In the majority of studies on feedback control of overhead cranes, the control input is assumed to be the actuator force applied to the trolley [6]–[11]. The partial feedback linearization [12] has been known to be useful to deal with the dynamics of the whole crane system including the trolley [7], [8], [10]. It is however not easy to apply to systems with complicated trolley dynamics, including the friction in the transmission and the actuators. In addition, many of such methods assume that the desired position signals are sufficiently smooth [6], [7], [9].

In contrast, some studies [3], [4], [13]–[16] focus on overhead crane systems of which the trolley is position-controlled.

The authors are with Graduate School of Advanced Science and Engineering, Hiroshima University, 1-4-1 Kagamiyama, Higashi-Hiroshima, Hiroshima 739-8527, Japan. The corresponding author is Ryo Nishimoto (e-mail: nishimoto@mdl.hiroshima-u.ac.jp).

Such methods are practically more convenient because many industrial actuators are integrated with optimized high-gain position controllers. In such methods, one can assume that the commanded position is accurately achieved as far as it is within the hardware limits. This means that position-commanding controllers need to provide sufficiently smooth position command, i.e., with its first and second derivatives being appropriately bounded. Model predictive control (MPC) is a convenient tool to account for the bounds of the velocity and acceleration [15], [17], but it is computationally costly and requires accurate dynamics model of the system.

This paper proposes a feedback-based anti-sway controller that gives position commands to the trolley. It assumes that the swing angle is measured by a sensor and that the trolley is accurately position-controlled. The controller incorporates an integral-like term of the measured sway angle to suppress the payload oscillation. It also imposes explicit upperbounds on the first and second derivatives of the position command. Due to these features, the controller is applicable to both human-operated systems and autonomous systems. The effectiveness of the proposed method is illustrated by some experimental results using a laboratory setup.

The integral-like term to damp the payload sway is a main feature of the presented controller. Some previous studies [6], [7], [9] employed the time integral of the sway angle to suppress the oscillation, but it can results in a steady-state offset in the trolley position even after the payload sway is settled. In the presented controller, the integral term is implemented in a modified way so that the offset reduces to zero almost in finite time once the payload sway is settled.

The rest of this paper is organized as follows. Section II provides some mathematical preliminaries. Section III shows the proposed controller and algorithm, and provides stability analysis. Section IV presents some experimental results. Section V shows an additional modification to the controller and some experimental results. Section VI concludes this paper.

II. MATHEMATICAL PRELIMINARIES

This paper uses the following notations:

$$\mathrm{sgn}(x) \triangleq \begin{cases} x/|x| & \text{if} \quad x \neq 0 \\ [-1, 1] & \text{if} \quad x = 0 \end{cases} \tag{1}$$

$$\mathrm{sat}_A(x) \triangleq \begin{cases} -A & \text{if} \quad x \leq -A \\ x & \text{if} \quad |x| < A \\ A & \text{if} \quad x \geq A \end{cases} \tag{2}$$

$$\mathcal{N}_{[-A,A]}(x) \triangleq \begin{cases} (-\infty, 0] & \text{if} \quad x = -A \\ 0 & \text{if} \quad |x| < A \\ [0, \infty) & \text{if} \quad x = A \\ \emptyset & \text{if} \quad |x| > A \end{cases} \tag{3}$$

$$\text{gsat}(a,x,b) \triangleq \begin{cases} a & \text{if} \quad x \le a \\ x & \text{if} \quad a < x < b \\ b & \text{if} \quad x \ge b \end{cases} \qquad (4)$$

$$\text{ssq}(x,\varepsilon) \triangleq \text{sgn}(x)(\sqrt{|x|+\varepsilon} - \sqrt{\varepsilon}) \qquad (5)$$

where $A > 0$, $a \le b$, and $\varepsilon \ge 0$. The set-valued functions sgn and $\mathcal{N}$ are referred to as the set-valued sign function and the normal cone [18], respectively. The single-valued functions sat and gsat are the saturation function and a generalized saturation function, respectively. The single-valued function ssq can be referred to as a relaxed sign-preserving square root, which is Lipschitz for all x if $\varepsilon > 0$ and reduces to the sign-preserving square root, which is non-Lipschitz at $x = 0$, if $\varepsilon = 0$.

The functions sgn, sat, and $\mathcal{N}$ satisfy the following relations:

$$y \in A\,\text{sgn}(x - y) \iff y = \text{sat}_A(x) \qquad (6)$$

$$y \in x - \mathcal{N}_{[a,b]}(y) \iff y = \text{gsat}(a,x,b). \qquad (7)$$

These relations can be proven as follows:

$$
\begin{aligned}
&y \in \text{sgn}(x - y) \\
&\iff ((y = -A) \wedge (x - y < 0)) \vee ((y \in [-A, A]) \\
&\quad \wedge (x - y = 0)) \vee ((y = A) \wedge (x - y > 0)) \\
&\iff ((y = -A) \wedge (x < -A)) \vee ((|y| < A) \\
&\quad \wedge (y = x)) \vee ((y = A) \wedge (x > A)) \\
&\iff y = \text{sat}_U(x). \qquad (8) \\
&y \in x - \mathcal{N}_{[a,b]}(y) \\
&\iff ((y \in x - (-\infty, 0]) \wedge (y = a)) \\
&\quad \vee ((y = x) \wedge (a < y < b)) \\
&\quad \vee ((y \in x - [0, \infty)) \wedge (y = b)) \\
&\iff ((y = a) \wedge (x \in (-\infty, a])) \\
&\quad \vee ((a < x < b) \wedge (y = x)) \\
&\quad \vee ((y = b) \wedge (x \in [b, \infty))) \\
&\iff ((y = a) \wedge (x \le a)) \vee ((a < x < b) \\
&\quad \wedge (y = x)) \vee ((y = b) \wedge (x \ge b)) \\
&\iff y = \text{gsat}(a, x, b). \qquad (9)
\end{aligned}
$$

When $a = -A$ and $b = A$, (7) reduces to the following:

$$y \in x - \mathcal{N}_{[-A,A]}(y) \iff y = \text{sat}_A(x). \qquad (10)$$

The function ssq satisfies the following:

$$\frac{\partial\,\text{ssq}(x,\varepsilon)}{\partial x} = \frac{1}{2\sqrt{|x|+\varepsilon}}. \qquad (11)$$

We also have the following relation:

$$
\begin{aligned}
&y - u = -A\,\text{ssq}(y, \varepsilon) \\
&\quad \iff y = u - A\,\text{ssq}(u, (\sqrt{\varepsilon} + A/2)^2) \qquad (12)
\end{aligned}
$$

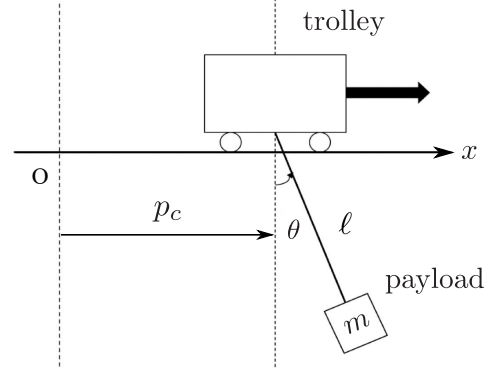for $A > 0$. It can be verified by checking all possible signs of y and u.

Fig. 1. Dynamics model of a 2-D overhead crane.

III. PROPOSED METHOD

A. Dynamics Model of 2-D overhead crane

The dynamics model of a two-dimensional (2-D) overhead crane is shown in Fig. 1. Considering the kinetic energy, the potential energy, and the Lagrangian of the payload, one can straightforwardly derive the equation of motion of the payload as follows:

$$m\ell^2\ddot{\theta} + mg\ell\sin\theta + m\ell\ddot{p}_c\cos\theta = \ell f \qquad (13)$$

where p_c is the trolley position, θ is the payload swing angle, m is the payload mass, ℓ is the wire length, g is the gravitational acceleration, and f is the external force acting on the payload. We assume that the trolley accurately follows the command position from the controller, and thus the trolley position and the command position are both represented by p_c. We also assume that the wire length ℓ is constant, and that the swing angle $\theta \in [-\pi/2, \pi/2]$ is measured by an angle sensor.

From (13), one can see that the swing of the crane system is caused by the acceleration of the trolley. This paper aims to present a controller of the position-commanding type; i.e., p_c is treated as the control input. Its first and second derivatives, $\dot{p}_c$ and $\ddot{p}_c$, need to be designed so that they do not exceed the actuator capacity.

B. Proposed controller

We propose a controller of which the continuous-time representation is written as follows:

$$\dot{p}_r = \text{sat}_U\left((p_t - p_r)/H\right) \qquad (14a)$$

$$\dot{\rho} \in \theta - \lambda\,\text{ssq}(\rho, \varepsilon) - \mathcal{N}_{[-Z/K, Z/K]}(\rho) \qquad (14b)$$

$$p_p = p_r + K\rho \qquad (14c)$$

$$p_c \in p_p - \mathcal{N}_{[-V,V]}(\dot{p}_c) - \mathcal{N}_{[-A,A]}(\ddot{p}_c). \qquad (14d)$$

The inputs to this controller are the desired position p_d and the measured sway angle θ, and the output is the position command p_c to the trolley. The variables p_r, ρ, and p_p are internal state variables of the controller. The controller parameters are U, H, λ, Z, K, V, and A, which are all positive constants. The parameter ε is a small non-negative constant, which can be zero in practice, as will be discussed in Section III-E.
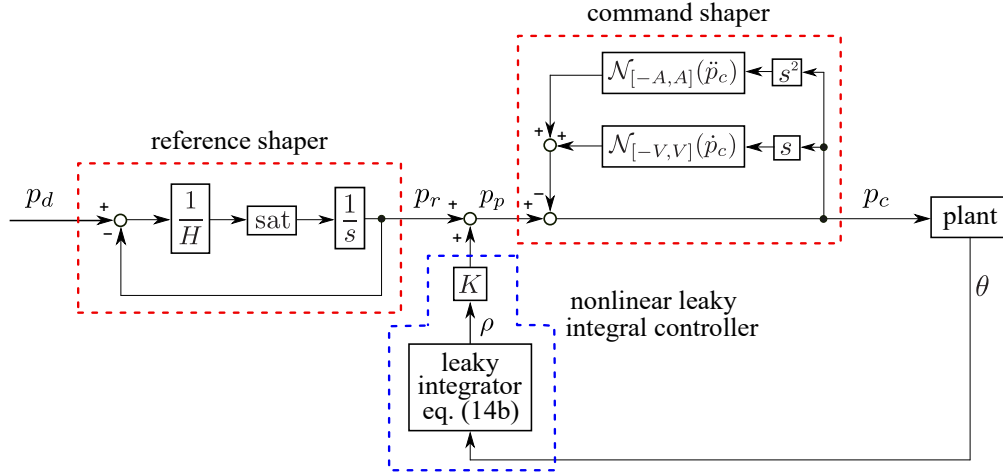
Fig. 2. Block diagram of the proposed controller.

The block diagram of this control law is illustrated in Fig. 2. It can be divided into three parts. The first part is the reference shaper, which corresponds to (14a). This part translates the desired position p_d to a reference position p_r. With (14a), the reference position p_r exponentially converges to p_d with the time constant H, and its rate of change is upperbounded by U. These parameters can be adjusted by considering how slow the reference position p_r should be.

The second part is the nonlinear leaky integral controller, which corresponds to (14b)(14c). The sway angle θ is given to the 'nonlinear leaky integral' (14b) and its output ρ is added to the reference position p_r to provide the secondary reference position p_p. As will be detained in the next Section III-C, the quantity ρ acts similarly to the time integral of θ but ρ decays to zero when θ is settled into zero. In addition, due to the effect of the third term in the right-hand side of (14b), ρ is upperbounded by the parameter Z.

The last part is the command shaper, which corresponds to (14d). The command shaper translates the secondary reference position p_p into the position command p_c by imposing upperbounds on its first and second derivatives. It prevents the controller from commanding the trolley beyond its capabilities.

C. Nonlinear Leaky Integral controller

The nonlinear leaky integrator (14b), which also appears in Fig. 2, is motivated by some previous studies [6], [7], [9], in which the integral term is used to damp the oscillation. Let us consider the controller (14) in the case where no quantities are saturated, (14b) is replaced by an ordinary integrator. Then, it can be simplified into the following:

$$\dot{\rho} = \theta \tag{15a}$$
$$p_c = p_r + K\rho. \tag{15b}$$

Substituting them into the plant dynamics (13) results in the following:

$$\ell\ddot{\theta} + K\dot{\theta}\cos\theta + g\sin\theta = f/m - \ddot{p}_r\cos\theta. \tag{16}$$

It implies that the term proportional to K acts as a damping term for the swing angle θ, and thus a large K value contributes to a quick convergence of θ to zero.

One problem of the integral controller (15) is that, even after the swing angle θ is settled into zero, there may remain a steady-state offset $K\rho$ between the trolley position p_c and the reference position p_r. The previous studies [6], [7], [9] have shown that ρ converges to zero if the initial sway angle is zero and there is no disturbance, but it would remain non-zero otherwise. One remedy for this drawback is to add a feedback term to (15a) as follows:

$$\dot{\rho} = \theta - \lambda_1\rho \tag{17}$$

where $\lambda_1 > 0$ is a positive constant. The dynamics (17) can be said to be a linear leaky integrator, which acts as an integrator in the frequency higher than $2\pi\lambda_1$ and the output ρ decays to zero with the time constant λ_1 once the input θ is settled to zero. The drawback of (17) is that the decay of ρ is asymptotic, which can be too slow in practice.

The presented controller (14) intends to adopt a nonlinear feedback term as follows:

$$\dot{\rho} = \theta - \lambda\operatorname{ssq}(\rho, \varepsilon). \tag{18}$$

With the dynamics (18), once θ is settled, $|\rho|$ decays to less than 4ε in finite time, and thus it contributes to a practically faster decay of ρ than (17). This feature can be explained as follows. Setting $\theta = 0$ with (18) results in the following:

$$\begin{aligned}
\frac{d|\rho|}{dt} &= -\lambda\operatorname{sgn}(\rho)\operatorname{ssq}(\rho, \varepsilon) \\
&= -\lambda\sqrt{|\rho| + \varepsilon} + \lambda\sqrt{\varepsilon} \\
&\leq -\lambda\sqrt{|\rho|} + \lambda\sqrt{\varepsilon} \\
&= -\lambda\sqrt{|\rho|}/2 - (\lambda/2)(\sqrt{|\rho|} - 2\sqrt{\varepsilon}). \tag{19}
\end{aligned}$$

Here, we should note that the solution of the differential equation $\dot{x} = -\lambda\sqrt{x}/2$ is $x = \max(0, \sqrt{x(t_0)} - \lambda(t-t_0)/4)^2$ for $t \geq t_0$ if $x(t_0) \geq 0$. Noting that (19) implies $d|\rho|/dt \leq -\lambda\sqrt{|\rho|}/2$ if $|\rho| \geq 4\varepsilon$, one obtains

$$|\rho| < \max(4\varepsilon, \sqrt{|\rho(t_0)|} - \lambda(t - t_0)/4)^2), \forall t \geq t_0 \tag{20}$$

from the comparison lemma (c.f., Section 3.4 of [19]). Therefore, $|\rho| \leq 4\varepsilon$ is achieved in finite time and the reaching time is less than $(4/\lambda)\max(0, \sqrt{|\rho(t_0)|} - 2\sqrt{\varepsilon})$.

D. Discrete-time implementation

The discrete-time form of the controller (14) is derived by the Backward (implicit) Euler discretization. Let T denotes the timestep size and k denotes the integer representing the discrete-time index. Although (14) includes many set-valued functions, such functions can be removed from its discrete-time representation by using some formula introduced in Section II.

First, the reference shaper (14a) can be discretized as follows:

$$\frac{p_{r,k} - p_{r,k-1}}{T} = \mathrm{sat}_U\left(\frac{p_{d,k} - p_{r,k}}{H}\right). \tag{21}$$

Using the relation (6), (21) can be rewritten as

$$\frac{p_{r,k} - p_{r,k-1}}{T} \in U\,\mathrm{sgn}\left(\frac{p_{d,k} - p_{r,k-1}}{T+H} - \frac{p_{r,k} - p_{r,k-1}}{T}\right) \tag{22}$$

and it can also be rewritten as follow:

$$p_{r,k} = \mathrm{sat}_U\left(\frac{p_{d,k} - p_{r,k-1}}{T+H}\right). \tag{23}$$

Thus, one can see that (23) is the discrete-time representation of the reference shaper (14a).

Next, the nonlinear leaky integrator (14b) can be discretized as follows:

$$\frac{\rho_k - \rho_{k-1}}{T} \in \theta_k - \lambda\,\mathrm{ssq}(\rho_k, \varepsilon) - \mathcal{N}_{[-Z/K, Z/K]}(\rho_k), \tag{24}$$

which can be rewritten as follows:

$$\rho_k - \rho_k^* \in -T\lambda\,\mathrm{ssq}(\rho_k, \varepsilon) - \mathcal{N}_{[-Z/K, Z/K]}(\rho_k) \tag{25a}$$

$$\rho_k^* \triangleq \rho_{k-1} + T\theta_k. \tag{25b}$$

By using (10) and (12), its equivalent form can be written as follow:

$$\rho_k = \mathrm{sat}_{Z/K}(a - T\lambda\,\mathrm{ssq}(a, (\sqrt{\varepsilon} + T\lambda/2)^2)). \tag{26}$$

Note that (26) can be seen as a closed-form solution of the algebraic constraint (24) with respect to ρ_k, and also as the discrete-time implementation of the nonlinear leaky integrator (14b). Although (14b) involves a set-valued function that cannot be computed directly, its discrete-time counterpart (26) does not.

The command shaper (14d) can be discretized as follows:

$$p_{c,k} \in p_{p,k} - \mathcal{N}_{[-V,V]}(v_{c,k}) - \mathcal{N}_{[-A,A]}(a_{c,k}) \tag{27a}$$

$$v_{c,k} = (p_{c,k} - p_{c,k-1})/T \tag{27b}$$

$$a_{c,k} = (v_{c,k} - v_{c,k-1})/T. \tag{27c}$$

Eliminating $p_{c,k}$ and $v_{c,k}$ from (27) yields the following:

$$a_{c,k} \in a_{c,k}^* - \mathcal{N}_{[\alpha_1, \alpha_2]}(a_{c,k}) - \mathcal{N}_{[-A,A]}(a_{c,k}) \tag{28}$$

where

$$a_{c,k}^* \triangleq (p_{p,k} - (p_{c,k-1} + Tv_{c,k-1}))/T^2 \tag{29a}$$

$$\alpha_1 \triangleq (-V - v_{c,k-1})/T \tag{29b}$$

$$\alpha_2 \triangleq (V - v_{c,k-1})/T. \tag{29c}$$

Regarding the right-hand side of (28), we can see the following:

$$\mathcal{N}_{[\alpha_1,\alpha_2]}(x) + \mathcal{N}_{[-A,A]}(x) = \mathcal{N}_{[\max(-A,\alpha_1),\min(A,\alpha_2)]}(x) \tag{30}$$

By using (29) and (7), one can see that (28) can be equivalently rewritten as follows:

$$a_{c,k} = \mathrm{gsat}(\max(-A, \alpha_1), a_{c,k}^*, \min(A, \alpha_2)). \tag{31}$$

This means that (31) is the closed-form solution of the algebraic constraint (28) with respect to $a_{c,k}$. One can see that the discrete-time implementation of the command shaper (14d) can be constructed from (31) to obtain $a_{c,k}$ and (27b) and (27c) to obtain $p_{c,k}$.

From these derivation, the algorithm of the proposed controller (14) can be written as follows:

$$p_{r,k} := p_{r,k-1} + T\,\mathrm{sat}_U\left(\frac{p_{d,k} - p_{r,k-1}}{T+H}\right) \tag{32a}$$

$$\rho_k^* := \rho_{k-1} + T\theta_k \tag{32b}$$

$$\rho_k := \mathrm{sat}_{Z/K}(\rho_k^* - T\lambda\,\mathrm{ssq}(\rho_k^*, (\sqrt{\varepsilon} + T\lambda/2)^2)) \tag{32c}$$

$$p_{p,k} := p_{r,k} + K\rho_k \tag{32d}$$

$$a_{c,k}^* := ((p_{p,k} - p_{c,k-1})/T - v_{c,k-1})/T \tag{32e}$$

$$a_{c,k} := \mathrm{gsat}\Big(\max\big(-A, (-v_{c,k-1} - V)/T\big),$$
$$a_{c,k}^*, \min\big(A, (-v_{c,k-1} + V)/T\big)\Big) \tag{32f}$$

$$v_{c,k} := v_{c,k-1} + Ta_{c,k} \tag{32g}$$

$$p_{c,k} := p_{c,k-1} + Tv_{c,k}. \tag{32h}$$

It should be noted that the algorithm (32) does not include any set-valued functions although its continuous-time representation (14) includes many such functions.

E. Stability Analysis

Behaviors of the whole system composed of the plant (13) and the controller (14) are now discussed. As can be seen in Fig. 2, the system can be seen as an open-loop combination of the reference shaper and a closed-loop subsystem. Thus, we here only focus on the closed-loop subsystem. In addition, for the simplicity of the discussion, we only consider the case where ρ, $\dot{p}_c$, and $\ddot{p}_c$ are not saturated. Then, the closed-loop subsystem can be written as follows:

$$\dot{\rho} = \theta - \lambda\,\mathrm{ssq}(\rho, \varepsilon) \tag{33a}$$

$$p_c = p_r + K\rho \tag{33b}$$

$$\dot{\theta} = \omega \tag{33c}$$

$$\ell\dot{\omega} = -g\sin\theta - \ddot{p}_c\cos\theta + f/m. \tag{33d}$$

In order to eliminate p_c from (33), let us derive $\ddot{p}_c$ from (33a) and (33b) as follows:

$$\ddot{p}_c = \ddot{p}_r + K\ddot{\rho}$$
$$= \ddot{p}_r + K\left(\dot{\theta} - \frac{\lambda\dot{\rho}}{2\sqrt{|\rho| + \varepsilon}}\right)$$
$$= \ddot{p}_r + \frac{K\lambda^2\,\mathrm{ssq}(\rho, \varepsilon)}{2\sqrt{|\rho| + \varepsilon}} - \frac{K\lambda\theta}{2\sqrt{|\rho| + \varepsilon}} + K\omega. \tag{34}$$

By substituting (34) into (33), one can obtain the state-space representation of the system as follows:

$$\dot{x} = F(x) + \begin{bmatrix} 0 \\ 0 \\ 1 \end{bmatrix} \frac{f/m - \ddot{p}_r \cos\theta}{\ell} \quad (35a)$$

where

$$x \triangleq [\rho, \theta, \omega]^T, \quad k \triangleq g/\ell, \quad c \triangleq K/\ell, \quad (35b)$$

$$F(x) \triangleq \begin{bmatrix} 1 \\ 0 \\ \dfrac{\lambda c}{2\sqrt{|\rho| + \varepsilon}} \end{bmatrix} (-\lambda \operatorname{ssq}(\rho, \varepsilon) + \theta)$$

$$+ \begin{bmatrix} 0 \\ \omega \\ -k \sin\theta - c\omega \cos\theta \end{bmatrix}. \quad (35c)$$

The closed-loop system (35), which is derived from (33), has the following property:

Theorem 1. *With the system* (35)*, the origin* $x = 0$ *is asymptotically stable if* $\varepsilon > 0$ *and* $f_d \equiv \ddot{p}_r \equiv 0$.

Proof. It follows from the fact that the matrix

$$\left. \frac{\partial F(x)}{\partial x} \right|_{x=0} = \begin{bmatrix} \dfrac{-\lambda}{2\sqrt{\varepsilon}} & 1 & 0 \\ 0 & 0 & 1 \\ \dfrac{-c\lambda^2}{4\varepsilon} & -k + \dfrac{c\lambda}{2\sqrt{\varepsilon}} & -c \end{bmatrix} \quad (36)$$

is Hurwitz if $\varepsilon > 0$. $\square$

Remark 1. The above result applies to all cases with arbitrarily small $\varepsilon > 0$ but does no with $\varepsilon = 0$. The stability of the case of $\varepsilon = 0$ may be able to be proven by using a nonsmooth Lyapunov function in a similar approach to that in [20].

Remark 2. The function ssq appears in (14b) in the continuous-time representation and in (32c) in the discrete-time algorithm. In (32c), the second argument of ssq is $(\sqrt{\varepsilon} + T\lambda/2)^2$. This means that, even if one choose $\varepsilon = 0$ in the continuous-time representation (14), the gradient of the ssq part in the discrete-time algorithm (32) is upperbounded by $1/(T\lambda)$. One can therefore infer that the aforementioned analysis approximately applies to the case of $\varepsilon = 0$ in the discrete-time domain, and setting $\varepsilon = 0$ would not cause problems in practice.

IV. EXPERIMENTS

A. Setup

The controller was tested with a laboratory setup shown in Fig. 3, which was composed of a single-axis linear motor, a trolley, and a payload. The trolley was attached to the slider part of the linear motor. An encoder with the resolution 3600 pulse/rev was used to measure the swing angle. The axis of the encoder was connected to the center of the pulley. The stroke of the linear motor was 0.35 m and its nominal maximum speed was 0.6 m/s. The mass of the payload was $m = 0.150$ kg and the length of the rope was $\ell = 0.38$ m. The linear motor was controlled by sending velocity (incremental
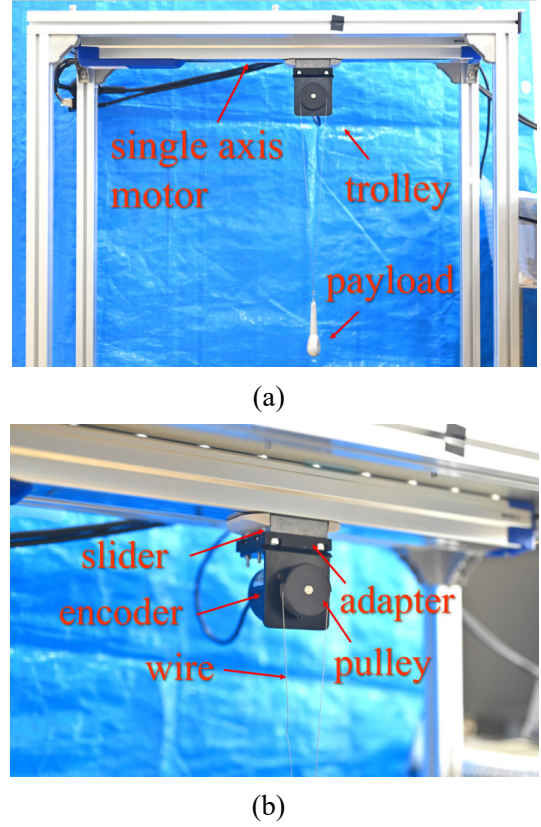

(a)

(b)

Fig. 3. Laboratory setup: (a) 2-D overhead crane, (b) configuration of the trolley.

position) signal from a PC running the Windows OS. We set the sampling interval to be $T = 0.002$ s. We used the following parameters in all experiments: $U = 0.4$ m/s, $H = 0.18$ s, $K = 3.2$ m/s, $\lambda = 0.3$ s$^{-1/2}$, $V = 0.5$ m/s, $A = 100$ m/s^2, and $Z = 0.16$ m.

The proposed controller was compared with another simple controller, which is written as follows:

$$\dot{p}_c = \operatorname{sat}_V \left((p_d - p_c)/H_w\right). \quad (37)$$

Note that it is exactly the same as (14a), which is the reference shaper part of the proposed controller. The controller (37) smooths the desired position p_d into the command position p_c. The discrete-time implementation of (37) is as follows:

$$p_{c,k} := p_{c,k-1} + T \operatorname{sat}_V \left(\frac{p_{d,k} - p_{c,k-1}}{T + H_w}\right). \quad (38)$$

Parameter H_w was set as $H_w = 0.6$ s so that it results in similar convergence behavior to that of the proposed controller.

B. Experiment I: Point-to-point (PTP) control

We investigated the anti-sway performance of the proposed controller (32) in comparison to the simple reference smoothing (38). At $t = 0$ s, the position of the trolley was set at $p_c = 0$ m and the payload was set at rest. The desired position was set to be $p_d = 0.25$ m for $t > 1$ s.

Results are shown in Fig. 4. It shows that the proposed controller effectively suppressed the oscillation after the trolley
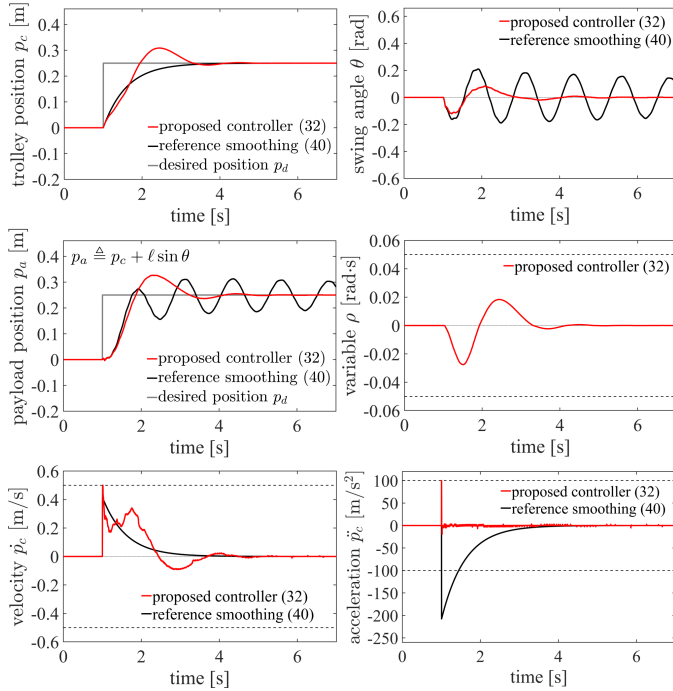
Fig. 4. Experiment I: point-to-point (PTP) control. The horizontal dotted lines indicate upper bounds of each variable.
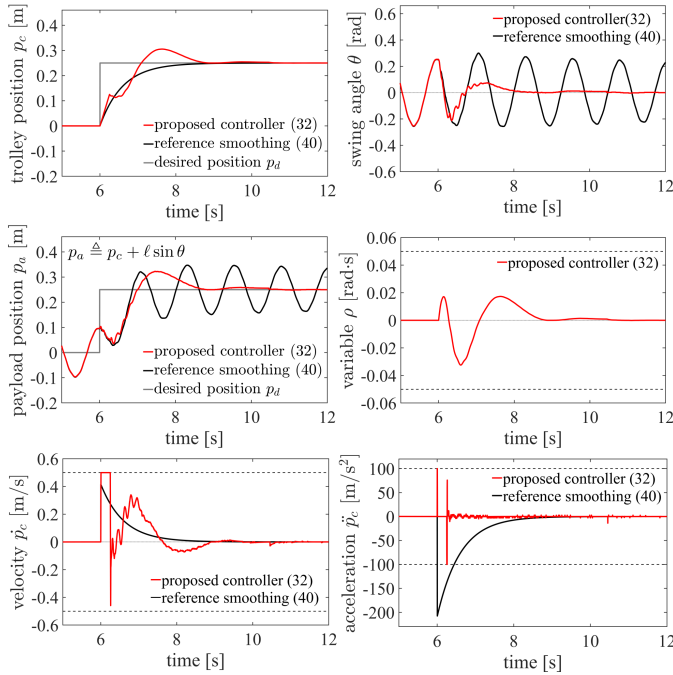

Fig. 5. Experiment II: PTP control with initial sway. The horizontal dotted lines indicate upper bounds for each variable.

reached the desired position under the velocity and acceleration constraints, i.e., $|\dot{p}_c| \leq V$ and $|\ddot{p}_c| \leq A$. Meanwhile, the payload continued oscillating with the simple reference smoothing (38). With the controller (38), the maximum swing angle was 0.210 rad ($\approx 12.0°$) at $t = 1.924$ s while it was -0.120 rad ($\approx -6.88°$) at $t = 1.226$ s with the proposed controller (32). The maximum swing angle was suppressed
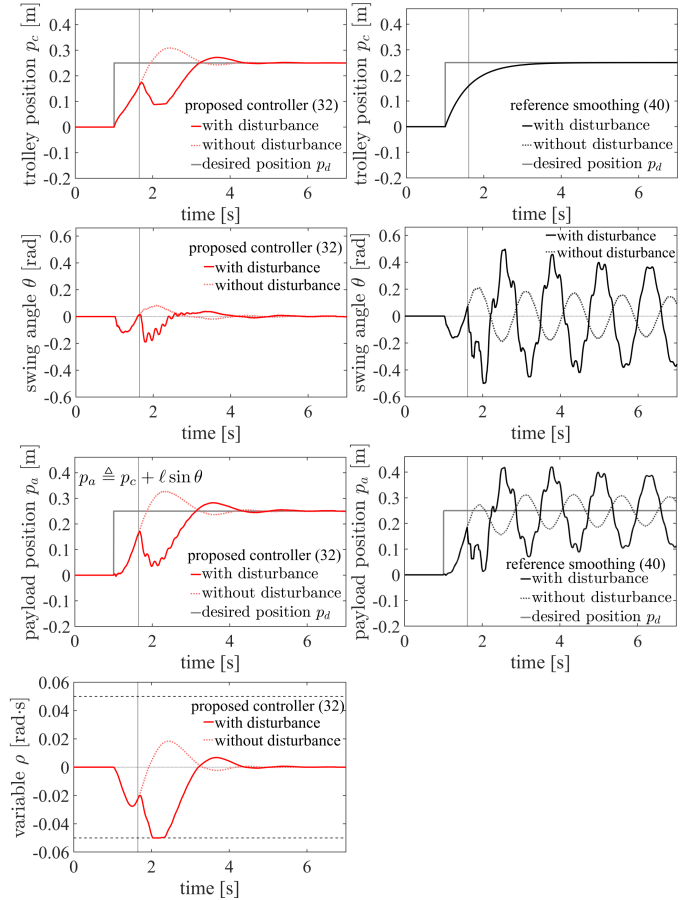
Fig. 6. Experiment III: PTP control under disturbance. The payload was hit by an external object at the time indicated by the gray vertical lines.

about 42.9% by the proposed controller.

One may notice that both trolley position p_c and the payload position $p_c + \ell \sin \theta$ exhibited overshoots before convergence. This point will be discussed in the next Section V.

C. Experiment II: PTP control with initial sway

We also performed a set of experiments to check the influence of the initial sway of the payload. At $t = 6$ s, the trolley was at $p_c = 0$ m and the payload was initially swaying. Then, the desired position was set to be $p_d = 0.25$ m for $t > 6$ s.

The results are shown in Fig.5. It shows that the proposed controller suppressed the swaying motion and made the trolley reach the desired position p_d under velocity and acceleration constraints. In contrast, with the reference smoothing (38), the swaying motion continued without decaying.

D. Experiment III: PTP control under disturbance

Another set of experiments was performed to test the influence of disturbance. The payload was at rest in the beginning, and the desired position p_d was set to be 0.25 s for $t > 0$, and in the middle of motion, the payload was hit by an external object.

Fig. 6 shows the results of the proposed controller (32) and the reference smoothing (38) where the payload was hit
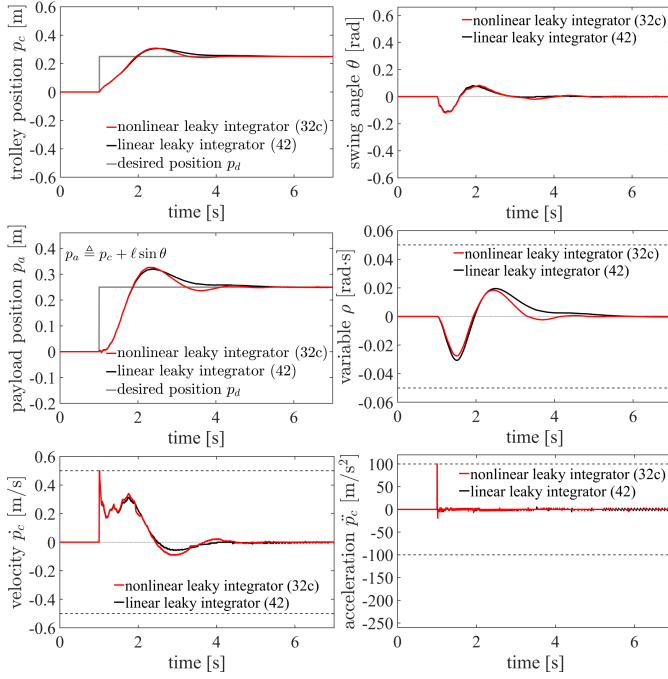
Fig. 7. Experiment IV: effects of the nonlinear leaky integral controller.

and was not hit. The gray vertical lines show the time at which the payload was hit. The results show that the proposed controller (32) suppressed the payload sway and that the trolley eventually reached the desired position p_d. With the reference smoothing (38), the payload sway increased due to disturbance.

E. Experiment IV: Nonlinearity of Leaky Integrator

Experiment IV was performed to illustrate the effect of the nonlinear function ssq introduced in the leaky integrator (14b). Recall that the nonlinear term involving the function ssq is intended to realize finite-time convergence while using a linear one would result in asymptotic convergence. For comparison, this experiment used the saturated linear leaky integrator of which the continuous-time representation was

$$\dot{\rho} \in \theta - \lambda_1 \rho - \mathcal{N}_{[-Z/K_1, Z/K_1]}(\rho). \qquad (39)$$

This integrator was implemented as the following algorithm:

$$\rho_k = \mathrm{sat}_{Z/K_1}((\rho_{k-1} + T\theta)/(1 + T\lambda_1)), \qquad (40)$$

which is the discrete-time representation of (39) obtained by the backward Euler discretization. This experiment compared the proposed algorithm (32) to the same algorithm with (32c) being replaced by (40). The parameters for (40) were carefully chosen as $K_1 = 2.3$ m/s and $\lambda_1 = 1.5$ s^{-1} so that it achieved a similar magnitude of the swing angle and overshoot to the proposed algorithm with the parameters used in other Experiments.

The results are shown in Fig. 7, which shows that the trolley position p_c settled to the desired position p_d faster with the nonlinear one (32c) than with the linear one (40). The settling time ($\pm$ 2%) of the nonlinear one (32c) was $t = 3.90$ s, and that of the linear one (40) was $t = 4.84$ s. With the linear one

(40), the convergence of ρ was slow especially near ρ, and it caused slower reaching of the trolley to the desired position p_d.

V. MODIFICATION OF CONTROLLER

Experimental results in the previous section show that the proposed controller (32) resulted in some overshoots in the trolley and payload positions. This feature may be seen as problematic in some applications. This section provides a variant of the controller (32) that prevents the overshoots. Its block diagram is shown in Fig. 8; the only difference is an add-on algorithm to provide an offset b to be added to the desired position p_d. This section details the add-on algorithm and shows some experimental results.

A. Modification: an Add-on Algorithm

The overshoot caused by the proposed controller (32) can be attributed to the fact that, when the trolley is decelerating before reaching the desired position p_d, the payload is pulled toward the desired position p_d by the inertial force. Therefore, one idea to avoid this situation is that the trolley should stop for a while before reaching the desired position.

A possible realization of this idea can be illustrated as in Fig. 9. When the desired position p_d is separated from the current trolley position p_c, an offset value b is added to p_c and the resultant value $p_t \triangleq p_d + b$ is used as a modified desired position. A while after the trolley p_c passes $p_d + b$, b is reduced to reach 0 in time T_2. This procedure should be initiated when the desired position p_d is settled, meaning that $|p_{d,k} - p_{d,k-1}|$ is small enough. Based on this idea, we propose the following algorithm to determine b:

$$B_k := \begin{cases} r(p_{c,k-1} - p_{d,k}) & \text{if } |p_{d,k} - p_{d,k-1}| > QT \\ B_{k-1} & \text{otherwise} \end{cases} \qquad (41a)$$

$$D_k := \begin{cases} 0 & \text{if } 0 \le B_k < p_{c,k-1} - p_{d,k} \\ 0 & \text{if } p_{c,k-1} - p_{d,k} < B_k \le 0 \\ D_{k-1} + T & \text{otherwise} \end{cases} \qquad (41b)$$

$$b_k := \begin{cases} B_k & \text{if } 0 \le D_k < T_1 \\ b_{k-1} - TB_k/T_2 & \text{if } T_1 \le D_k < T_1 + T_2 \\ 0 & \text{otherwise.} \end{cases} \qquad (41c)$$

With this algorithm, the inputs are p_d and p_c, the output is b_k, and the current values $\{p_{d,k}, B_k, D_k, b_k\}$ should be reused as $\{p_{d,k-1}, B_{k-1}, D_{k-1}, b_{k-1}\}$ in the next timestep. The parameters are $Q > 0$, $r \in (0,1)$, $T_1 > 0$, and $T_2 > 0$, which should be chosen appropriately. The variable D_k counts the time spent after p_c crosses $p_d + B_k$.

B. Experiments

We investigated the performance of the modified controller with the add-on algorithm (41) by using the experimental setup introduced in Section IV. The parameters were set as: $Q = 0.02$ m/s, $r = 0.25$, $T_1 = 0.25$ s, and $T_2 = 0.25$ s. The other parameters were set to the same values as those in Section IV.

Fig. 10 shows the results of PTP control from a resting position. The experimental conditions were identical to those
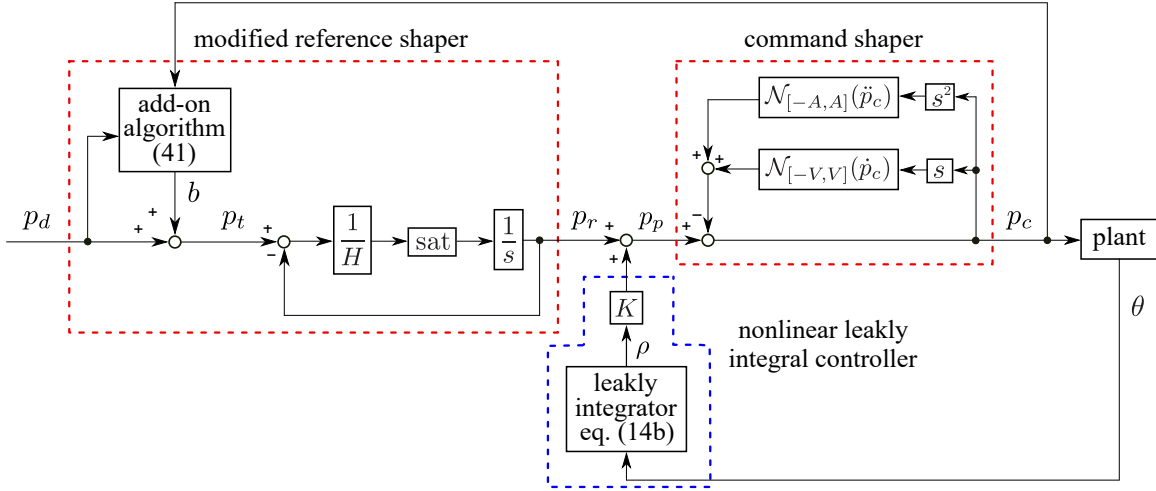
Fig. 8. Block diagram of the modified controller with the add-on algorithm (41).
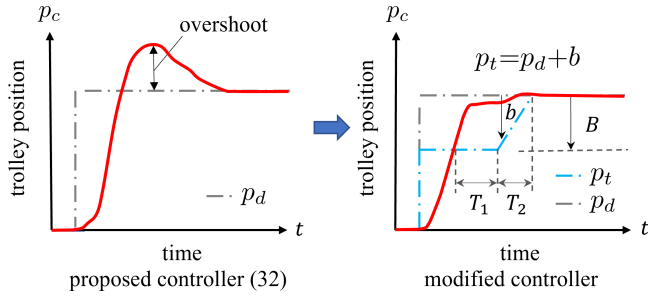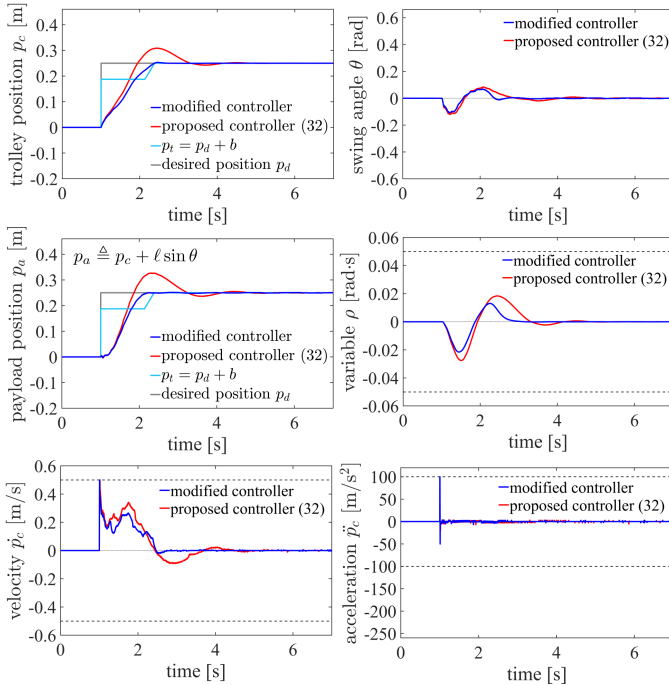

Fig. 9. Concept of the modified controller.

Fig. 10. PTP Control with the modified controller.

Fig. 11. PTP Control with initial sway with the modified controller.

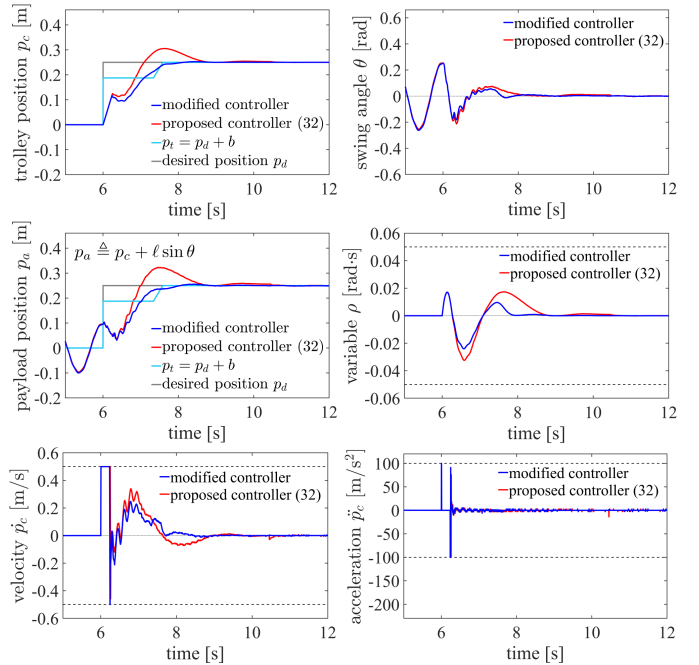of Experiment I in Section IV-B. It shows that the add-on algorithm (41) effectively reduced the overshoot and the settling time without causing an increase in the swing angle. With the original controller (32), the maximum overshoot was 0.05 m and the settling time (± 2 %) was $t = 3.90$ s. In contrast, with the add-on algorithm (41), they were reduced to 0.003 m and $t = 2.32$ s, respectively.

Fig. 11 shows the results of PTP control with an initial sway, which was performed in the same conditions as those of Experiment II in Section IV-C. It shows that the add-on algorithm (41) suppresses the overshoot even when the payload is swinging at the beginning of the motion.

Fig. 12 shows the results of PTP control under disturbance in the same conditions as Experiment III in Section IV-D. In these experiments, the payload was initially at rest, the desired position p_d was moved by 0.25 m at $t = 0$, and the payload was hit by an external object in the middle of the motion.
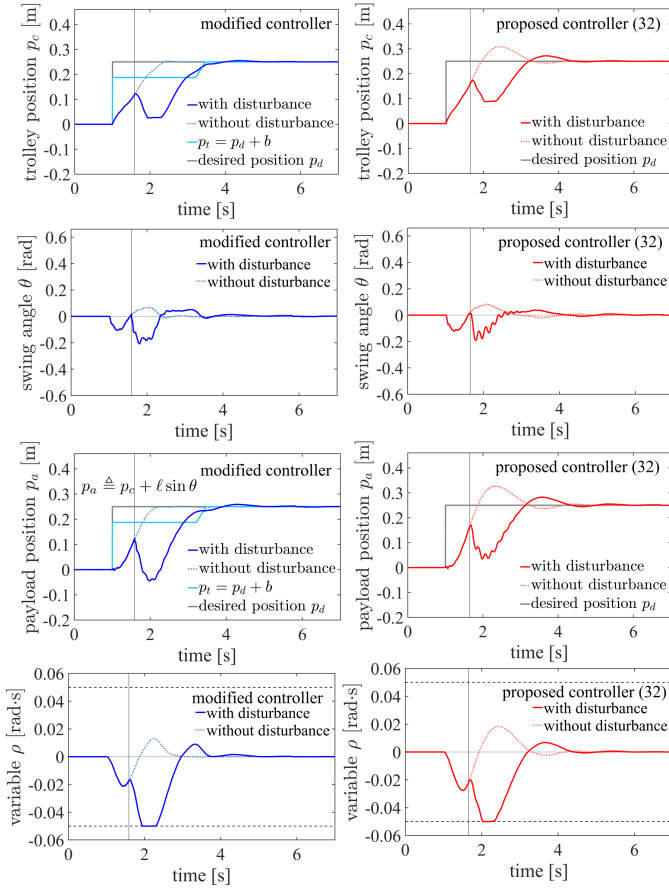
Fig. 12. PTP Control under disturbance with the modified controller. The payload was hit by an external object at the time indicated by the gray vertical lines.
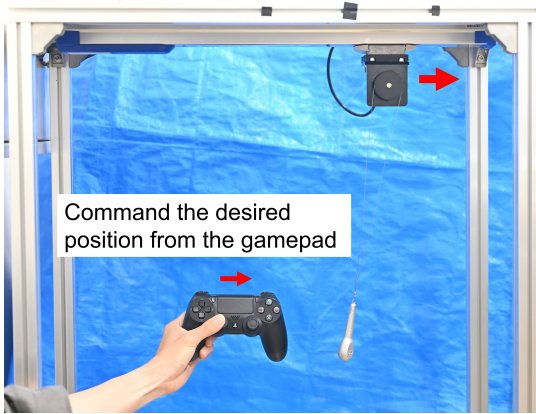

Fig. 13. Experimental setup of the human operation of the crane.

The results show that the add-on algorithm (41) suppresses the overshoot and oscillation even under disturbance, which is unpredictable to the controller.

We also performed an experiment in which the experimenter operated the setup through a gamepad as shown in Fig. 13. Here, the position of the gamepad stick was mapped to the desired position command p_d. The results are shown in Fig. 14. As can be seen in Fig. 14, the experimenter performed several back-and-forth motions slowly and rapidly, resulting in often discontinuous position commands. It can be seen that the
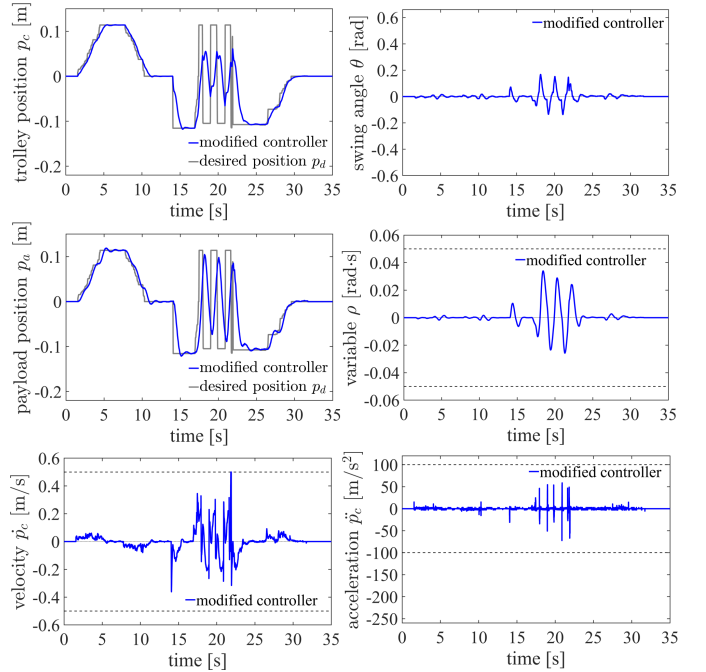

Fig. 14. Human operation of the crane with the modified controller. Note that the scale of the vertical axis of the trolley position p_c and payload position are not the same as those in other experiments.

method effectively suppressed the overshoot and sway even under highly variable position commands.

VI. CONCLUSION

This paper has proposed a position-commanding anti-sway controller for 2-D overhead cranes. It is for crane systems of which the trolleys are equipped with stiff low-level position controllers, and it requires the sensory information of the payload sway angle. The main feature of the controller is that upperbounds of velocity and acceleration can be explicitly specified by controller parameters. In addition, it employs a nonlinear integral-like term to damp the payload sway without causing an offset in the trolley position. The controller can be used even when the desired position commands are discontinuous and unpredictable, and thus it is usable for both human-operated and automatic cranes. The controller was validated with a laboratory setup. A small modification to the controller to suppress overshoots has also been presented.

Future work should address the inclusion of hoisting actions and the extension to three-dimensional cranes. In addition, the clarification of parameter tuning guidelines would also be necessary. Human factor analyses, such as those in [21], should also be sought to clarify better parameter settings that are suited for human-operated applications.

REFERENCES

[1] E. M. Abdel-Rahman, A. H. Nayfeh, and Z. N. Masoud, "Dynamics and control of cranes: A review," *Journal of Vibration and Control*, vol. 9, pp. 863–908, 2003.

[2] W. Singhose, D. Kim, and M. Kenison, "Input shaping control of double-pendulum bridge crane oscillations," *Transactions of ASME: Journal of Dynamic Systems, Measurement, and Control*, vol. 130, p. 034504, 2008.

[3] K. Alghanim, A. Mohammed, and M. Taheri Andani, "An input shaping control scheme with application on overhead cranes," *International Journal of Nonlinear Sciences and Numerical Simulation*, vol. 20, no. 5, pp. 561–573, 2019.

[4] A. Mohammed, K. Alghanim, and M. Taheri Andani, "An optimized non-linear input shaper for payload oscillation suppression of crane point-to-point maneuvers," *International Journal of Dynamics and Control*, vol. 7, no. 2, pp. 567–576, 2019.

[5] ——, "A robust input shaper for trajectory control of overhead cranes with non-zero initial states," *International Journal of Dynamics and Control*, vol. 9, no. 1, pp. 230–239, 2021.

[6] X. Li, X. Peng, and Z. Geng, "Anti-swing control for 2-D under-actuated cranes with load hoisting/lowering: A coupling-based approach," *ISA Transactions*, vol. 95, pp. 372–378, 2019.

[7] X. Wu and X. He, "Partial feedback linearization control for 3-D underactuated overhead crane systems," *ISA Transactions*, vol. 65, pp. 361–370, 2016.

[8] ——, "Nonlinear energy-based regulation control of three-dimensional overhead cranes," *IEEE Transactions on Automation Science and Engineering*, vol. 14, no. 2, pp. 1297–1308, 2017.

[9] R. Miranda-Colorado and L. T. Aguilar, "A family of anti-swing motion controllers for 2D-cranes with load hoisting/lowering," *Mechanical Systems and Signal Processing*, vol. 133, p. 163253, 2019.

[10] L. A. Tuan, S.-G. Lee, V.-H. Dang, S. Moon, and B. Kim, "Partial feedback linearization control of a three-dimensional overhead crane," *International Journal of Control, Automation, and Systems*, vol. 11, no. 4, pp. 718–727, 2013.

[11] N. Sun, Y. Fang, H. Chen, and B. He, "Adaptive nonlinear crane control with load hoisting/lowering and unknown parameters: Design and experiments," *IEEE/ASME Transactions on Mechatronics*, vol. 20, no. 5, pp. 2107–2119, 2015.

[12] M. W. Spong, "Partial feedback linearization of underactuated mechanical systems," in *Proceedings of the 1994 IEEE/RSJ International Conference on Intelligent Robots and Systems*, 1994, pp. 314–321.

[13] M. Giacomelli, F. Padula, L. Simoni, and A. Visioli, "Simplified input-output inversion control of a double pendulum overhead crane for residual oscillations reduction," *Mechatronics*, vol. 56, pp. 37–47, 2018.

[14] M. Giacomelli, M. Faroni, D. Gorni, A. Marini, L. Simoni, and A. Visioli, "MPC-PID control of operator-in-the-loop overhead cranes: A practical approach," in *Proceedings of International Conference on Systems and Control*, 2018, pp. 321–326.

[15] M. Giacomelli, D. Colombo, M. Faroni, O. Schmidt, L. Simoni, and A. Visioli, "Comparison of linear and nonlinear MPC on operator-in-the-loop overhead cranes," in *Proceedings of IEEE International Conference on Control, Mechatronics and Automation*, 2019, pp. 221–225.

[16] A. Mohammed, K. Alghanim, and M. Taheri Andani, "An adjustable zero vibration input shaping control scheme for overhead crane systems," *Shock and Vibration*, vol. 2020, p. 7879839, 2020.

[17] M. Giacomelli, M. Faroni, D. Gorni, A. Marini, L. Simoni, and A. Visioli, "Model predictive control for operator-in-the-loop overhead cranes," in *Proceedings of IEEE International Conference on Emerging Technologies and Factory Automation*, 2018, pp. 589–596.

[18] R. Kikuuwe and B. Brogliato, "A new representation of systems with frictional unilateral constraints and its Baumgarte-like relaxation," *Multibody System Dynamics*, vol. 39, no. 3, pp. 267–290, 2017.

[19] H. K. Khalil, *Nonlinear Systems*, 3rd ed. Upper Saddle River: Prentice Hall, 2002.

[20] J. A. Moreno and M. Osorio, "Strict Lyapunov functions for the super-twisting algorithm," *IEEE Transactions on Automatic Control*, vol. 57, no. 4, pp. 1035–1040, 2012.

[21] D. Kim and W. Singhose, "Performance studies of human operators driving double-pendulum bridge cranes," *Control Engineering Practice*, vol. 18, pp. 567–576, 2010.